Eur. Phys. J. D **45**, 289–294 (2007)
DOI: 10.1140/epjd/e2007-00241-3

THE EUROPEAN PHYSICAL JOURNAL D

First-principles study of structural evolution of medium-sized Si_N clusters ($41 \leqslant N \leqslant 50$) within stuffed fullerene cages

J. Wang[1], J. Zhao[2,a], L. Ma[2], and G. Wang[1,b]

[1] National Laboratory of Solid State Microstructures and Department of Physics, Nanjing University, Nanjing 210093, P.R. China
[2] State Key Laboratory of Materials Modification by Laser, Electron, and Ion Beams, School of Physics and Optoelectronic Technology and College of Advanced Science and Technology, Dalian University of Technology, Dalian 116024, P.R. China

Received 4 February 2007 / Received in final form 14 May 2007
Published online 27 July 2007 –

Abstract. The stuffed fullerene structures of medium-sized Si_N ($41 \leqslant N \leqslant 50$) clusters have been systemically studied using the all-electron density functional theory with gradient correction. For each cluster size, fullerene cages with different topologies and filled by different number of atoms were constructed and optimized to find the lowest-energy structure. The core atoms filled in the fullerene cages tend to form cage-like structures that resemble structural character of bulk diamond fragments. The size-dependent physical properties such as binding energies, electronic gaps, and ionization potentials have been discussed. Si_{45} exhibits relatively higher stability that can be associated with the low chemical reactivity observed by experiment.

PACS. 36.40.Mr Spectroscopy and geometrical structure of clusters – 61.46.+w Nanoscale materials – 61.48.+c Fullerenes and fullerene-related materials

1 Introduction

Over the past two decades, investigation of the structures and relative stability of medium-sized silicon clusters Si_N (N = 20–100) has become an attractive area. Considerable effort has been devoted to the determination of the ground-state geometric structures, namely, the global minima as a function of the cluster size N. For the smallest Si_N clusters with $N \leqslant 7$, their structures have been determined by ab initio calculations with aid of experimental information such as anion photoelectron spectroscopy [1], Raman [2] and infrared [3] spectra, and high-resolution photoelectron [4], etc. It was found that the geometric structures of the small Si_N clusters are quite different from fragments of a bulk diamond lattice [5,6]. As the size of clusters increases sufficiently, it is natural to expect that the silicon clusters would possess a bulk-like diamond structure with a reconstructed surface. Thus, understanding the size evolution of cluster geometry and exploring the transition toward the diamond structure are very important issues in the study of silicon clusters and nanostructures.

In the medium-sized region, ionic mobility experiments have revealed an crucial structural transition from prolate to near-spherical for silicon cation (Si_N^+) and anion (Si_N^-) clusters of $24 < N < 30$ [7]. Recently, such structural transition has also been confirmed by experimental/simulated [8] and theoretical [9,10] studies. Above the transition size, most of the observed cluster properties such as binding energies [11,12], ionization potentials [13], photoelectron spectra [14], and chemical reactivity [15] show smooth size-dependent behaviors, implying that the structures of the medium-sized Si_N ($N \geqslant 30$) clusters may follow the same growth pattern and the addition of one more atom will not result in dramatic reconstruction of cluster structure. On this transition size, the optical properties of the silicon clusters assembled films have also been investigated experimentally [16–18].

It is well-known that as the clusters size increases, determination of the true global minima on the potential energy surface (PES) becomes increasingly challenging because of the growing number of low-lying isomers. For the medium-sized Si_N clusters with $N \approx$ 11–30, different optimization methods such as genetic algorithm [19,20], basin-hopping techniques [21], and "big bang" methods [9], have been employed to perform an unbiased search for the global minimum on the PES. These calculations indicated that prolate supercluster structures using tricapped triangular prisms (TTP) model as building blocks are formed for Si_N with $N \approx$ 15–25, and that a structural transition from the prolate geometries to the more-spherical ones occurs for the medium-sized silicon clusters with $N \geqslant 25$.

[a] e-mail: zhaojj@dlut.edu.cn
[b] e-mail: ghwang@nju.edu.cn

Different from the carbon fullerene cages, hollow Si cage structures are unstable due to the lack of sp^2 hybridization of valence orbitals [22–25]. To stabilize the silicon cages, some additional atoms stuffed inside the cage are needed to saturate the dangling bonds on the silicon cage surface and to form sp^3 hybridization. Based on above considerations, a number of "handmade" endohedral cages have been constructed for the medium-sized silicon clusters (e.g., Si_{33}, Si_{36}, Si_{39}, Si_{40}, and Si_{45}) [26–32]. Recently, combining unbiased genetic algorithm (GA) search at semi-empirical nonorthogonal tight-binding (NTB) level and biased local optimization using density functional theory, Yoo et al. [33] have systematically studied the structures of the medium-sized Si_N clusters with $N = 27$–39. They found that silicon atoms form stuffed cage configurations within this size range and the outer cages mimic the fullerene cages of carbon clusters. Further studies on the structures of the medium-sized Si_N clusters (e.g., Ref. [10] for $N = 21$–30; Ref. [32] for $N = 40$; Ref. [34] for $N = 40$, 45 and 50; Ref. [35] for $N = 30$–39; and Ref. [36] for $N = 31$–40, 45) revealed that the endohedral silicon cages are the generic structural motif of the medium-sized Si_N clusters. So far, most of these previous works focused on Si_N with $N \leqslant 40$. For larger clusters in the size range of $41 \leqslant N \leqslant 50$, there have been a number of studies on Si_{45} [26,29,32–34,36–38] and few on Si_{50} [34]. Hence, it is necessary to conduct more comprehensive study on Si_N ($41 \leqslant N \leqslant 50$) clusters to understand the structural evolution. In particular, in the series works on Si_N ($N \leqslant 40$) clusters [32–36], main attentions have been focused on the outer cages configurations for the endohedral fullerene structures. As the cluster become larger, the interior silicon atoms within the cages would gradually form some kinds of core structure. Thus, how do the core structures evolve for the stuffed fullerene silicon clusters in the size range of $41 \leqslant N \leqslant 50$? In this paper, we carry out all-electron DFT calculations to study the medium-sized Si_N ($41 \leqslant N \leqslant 50$) clusters within structural motif of endohedral fullerene cages and examine the geometric structures of the core atoms in detail.

2 Computational procedure

In this work, the medium-sized Si_N clusters ($41 \leqslant N \leqslant 50$) within structural motifs of endohedral fullerene cages were studied using density functional theory (DFT). At the beginning, stuffed fullerene cages of different topologies and with different filling/cage ratios were constructed for Si_N ($41 \leqslant N \leqslant 50$). The initial structures of the fullerene cages were directly taken from those for carbon fullerenes in the Fullerene Structure Library [39] after a rescaling the bond length by a factor of 1.65. In a previous work [33], an unbiased search of global minima of medium-sized silicon clusters with $N = 29$–39 using the genetic algorithm demonstrated that most of the lowest-energy structures of silicon clusters exhibit fullerene-like cages which contain only pentagonal and hexagonal rings. Therefore, to reduce the number of structural isomers, here we considered all possible topologies for the classical fullerene cages (only containing five-membered and six-membered rings) for each size of outer cage. For the fullerene cages with 34, 36, 38, 40, and 42 surface atoms, we considered 6, 15, 17, 40, and 45 isomers, respectively. Similar to previous work [35], a suitable amount of silicon atoms were uniformly filled into the hollow silicon cages. These "hand-made" structural isomers were then optimized using all-electron density functional theory implemented in the DMol program [40]. We used a double numerical basis including d-polarization function (DND) and adopted the generalized gradient approximation (GGA) with Perdew-Burke-Ernzerhof (PBE) parameterization to describe the exchange-correlation interaction [41]. In DFT calculations, all the structures were fully optimized without any symmetry constraint. The convergence criteria for the gradient force and the total energy were set to 0.002 Hartree/Å and 10^{-6} Hartree, respectively. Using the present computational scheme, the values of the bulk silicon have been calculated. For the bulk silicon, the current computational scheme predicts the cohesive energy, equilibrium lattice constant and band gap 4.58 eV/atom, 5.47 Å and 0.68 eV respectively, which fairly close to experiments (4.63 eV/atom, 5.43 Å and 1.11 eV) [42]. These computed values are completely same as our recent DFT-PBE results [32]. It is well known that standard DFT approaches at LDA or GGA level significantly underestimate the band gap of semiconductor materials. Therefore, the present computational scheme can give a credible description of the medium-sized Si_N clusters ($41 \leqslant N \leqslant 50$) within stuffed fullerene cages.

3 Results and discussion

Using the computational approach described above, we have optimized a number of structural isomers for each size of Si_N ($41 \leqslant N \leqslant 50$) clusters with different possible combination of outer fullerene cages and endohedral filling atoms. For example, we considered 21 isomers for Si_{41}, while the number of isomers increases to 85 for Si_{50}. The lowest-energy endohedral fullerenes for Si_N ($41 \leqslant N \leqslant 50$) are shown in Figure 1, in which the endohedral atoms are highlighted in green color. To examine the structural evolution of the core atoms, we removed the outer cage atoms and only plotted the core configurations in Figure 3. The filling/cage combination, binding energies (E_b), vertical ionization potentials (VIPs) and electronic gaps between highest occupied molecular orbital-lowest unoccupied molecular orbital (HOMO-LUMO) for the lowest-energy endohedral structures are summarized in Table 1. Using a cutoff value of 2.65 Å (same in Ref. [35]), we calculated the average coordination numbers (CN) for the lowest-energy endohedral fullerene structures, which are also given in Table 1.

3.1 Structures of silicon clusters

As shown in Table 1 and Figure 1, the optimal filling/cage ratio for endohedral fullerene structures of Si_{41}, Si_{42}, Si_{43},

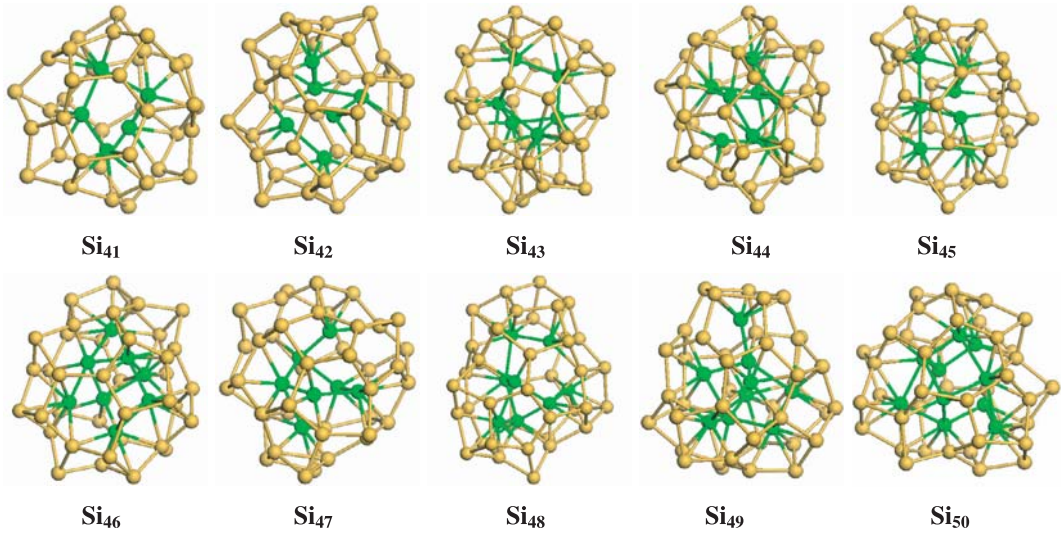

Fig. 1. (Color online) Lowest-energy endohedral fullerene structures for medium-sized Si_N ($41 \leqslant N \leqslant 50$) clusters. The endohedral atoms are highlighted in green color and the atoms on the outer cage in yellow color.

Table 1. Optimal filling and/or cage combination (Si_m@Si_n), binding energy (E_b) per atom, vertical ionization potential (VIP), HOMO-LUMO gap for the lowest-energy structures from our theoretical calculations. The average CN was calculated using a 2.65 Å cutoff.

Si_N	Si_m@Si_n	E_b (eV/atom)	VIP(eV)	CN	Gap (eV)
Si_{41}	Si_5@Si_{36}	3.862	6.010	3.66	0.531
Si_{42}	Si_6@Si_{36}	3.865	6.019	3.76	0.551
Si_{43}	Si_7@Si_{36}	3.862	5.921	4.14	0.360
Si_{44}	Si_8@Si_{36}	3.873	6.011	3.96	0.530
Si_{45}	Si_7@Si_{38}	3.885	6.022	4.55	0.704
Si_{46}	Si_8@Si_{38}	3.873	5.866	4.26	0.491
Si_{47}	Si_7@Si_{40}	3.878	5.987	3.79	0.604
Si_{48}	Si_8@Si_{40}	3.879	5.904	4.00	0.437
Si_{49}	Si_9@Si_{40}	3.885	5.885	4.16	0.323
Si_{50}	Si_{10}@Si_{40}	3.888	5.881	4.40	0.467

Si_{44} clusters are Si_5@Si_{36}, Si_6@Si_{36}, Si_7@Si_{36}, Si_8@Si_{36}, respectively. It is interesting to find that the symmetry of original C_{36} fullerene cages varies from D_{2d} for Si_{41} to C_2 for Si_{42}, C_1 for Si_{43}, and C_2 for Si_{44}. All of the optimized cluster configurations are spherical-like.

Among the Si_N clusters in the size range of $N = 41$–50, Si_{45} has received most intensive attention [26,29,30,33, 34,36–38] due to its unusually low chemical reactivity observed in experiment [43]. From our calculations, the optimal outer fullerene cage is Si_{38} for the Si_{45} cluster, and the corresponding original C_{38} fullerene cage has C_2 symmetry. The obtained stuffing/cage combination Si_7@Si_{38} for Si_{45} is in agreement with the previous results [34,36]. In reference [36], Zeng's group predicted a stuffing/cage combination of Si_5@Si_{40} using BLYP functional and Si_7@Si_{38} using PBE functional for Si_{45} cluster.

For the larger Si_N clusters ($N = 46$–50), the size of optimal outer fullerene cages are 38 for Si_{46}, and 40 for the rest. The original C_{38} fullerene cage for Si_{46} has no symmetry (C_1), while symmetries of the original C_{40} fullerene cages for Si_{47}, Si_{48}, Si_{49}, and Si_{50} are C_2, C_s, C_s, and C_1, respectively. Again, these lowest-energy endohedral fullerene cages are spherical-like.

3.2 Size dependence of binding energy, vertical ionization potentials and HOMO-LUMO gap

To understand the evolution behavior from microscopic atoms to bulk solids, it is important to discuss the size dependence of physical properties for the clusters. On the other hand, identification of the generic structural features not only can dramatically reduce computation cost for first-principles evaluation of the potential-energy surface but also can provide additional physical insight into growth patterns of the medium-sized clusters [10].

In Figure 2, the theoretical and experimental binding energies [11] per atom (Fig. 2a) and HOMO-LUMO gap (Fig. 2b) of Si_N clusters are plotted as function of cluster size. As shown in Figure 2a, the computed binding energy increases gradually with increasing cluster size, which is an essential requirement for identifying stable medium-sized clusters. Compared to experimental data [11], our theoretical calculations systematically underestimate the binding energies by about 0.2 eV. Thus, if we shift the experimental binding energies [11] by −0.2 eV, satisfactory agreement can be found between theory and experiment.

In both Figures 2a and 2b, we find distinct peaks in theoretical binding energy and HOMO-LUMO gap at Si_{45}, which is in accord with its unusually low chemical reactivity [43]. Experimentally, the energy gaps of silicon clusters were measured with scanning tunneling spectroscopy [44] and a finite gap up to 0.45 eV was estimated for the radius below 15 Å (about 40–50 atoms). The calculated HOMO-LUMO gaps oscillate around 0.45 eV with deviation of about 0.1 eV (see Tab. 1 and Fig. 1b). Thus, our computed gaps roughly agree with the experiment measurements [44].

The vertical ionization potentials (VIPs) defined by the differences of total energy of neutral and cationic clusters with the same lowest-energy configuration of the neutral state were also calculated and listed in Table 1. Si_{45}

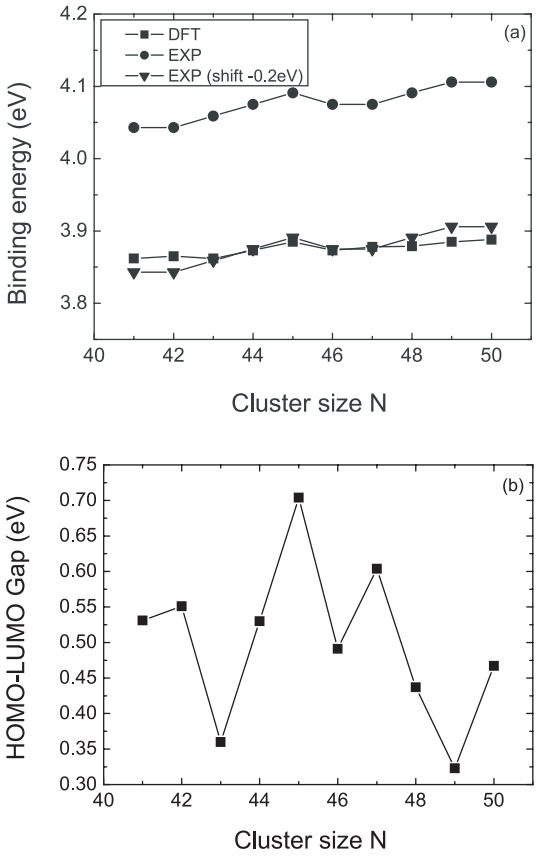

Fig. 2. Physical properties of Si_N clusters as function of cluster size N: (a) binding energy per atom (E_b). Square: our DFT calculation; circles: experimental data from reference [11]. Triangle: experimental data from reference [11] with a shift of −0.2 eV. (b) HOMO-LUMO gaps from our DFT calculations.

has the largest VIP value, which can be also associated with the higher chemical inertness. In previous experiment, the ionization potentials of Si_N cluster were determined by photoionization threshold measurements [13]. In the size range of $N = 41$–45, the measured IPs values are about 5.40–5.50 eV. Our calculation results are systematically higher than those experimental values by about 0.4 eV. From Table 1, one can see that the average CN generally increases as cluster size increases and they are all comparable to the CN = 4 for diamond lattice, although the average bond length is longer than the bulk value. Among the Si_N clusters, the CN for Si_{45} is larger than the others.

3.3 Core-filling atoms and stuffing/cage ratio

In Figure 3a, we display the structures of the core-filling atoms of the corresponding lowest-energy endohedral fullerene structures of Si_N with $N = 41$–50. Same atomic configurations of the core-filling atoms are plotted in Figure 3b with different aspects to compare with the bulk fragments. In Figure 3c, we present the structures of the two smallest bulk diamond fragments,

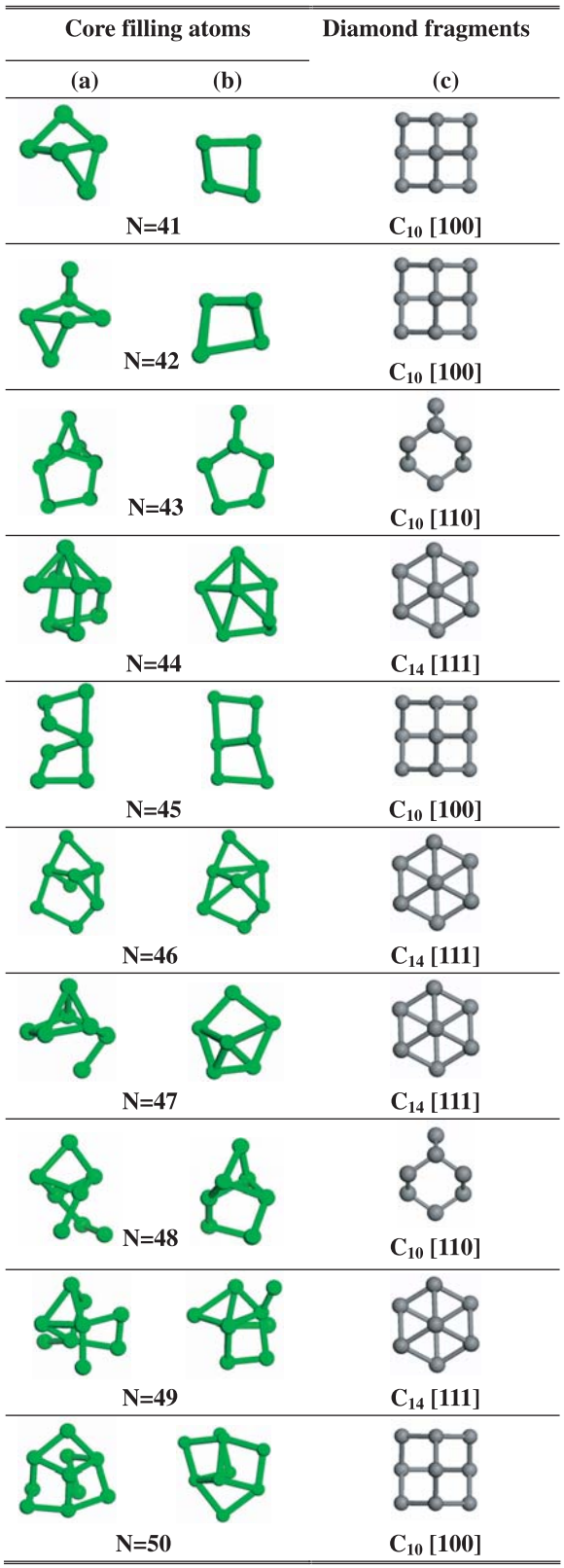

Fig. 3. (Color online) (a) Structures of the core-filling atoms within the lowest-energy endohedral fullerene structures of Si_N ($41 \leqslant N \leqslant 50$); (b) same structures of the core-filling atoms viewed from different aspects; (c) structures of diamond fragments like adamantine (C_{10}) and diamantine (C_{14}) viewed from different lattice orientations.

namely, adamantine [45] with 10-carbon atoms and diamantine [45] with 14-carbon atoms, along different lattice orientations. From Figure 3a, one can see that the core-filling atoms tend to form cage-like structures as the cluster size increases. In particular, the inner cores of Si_{44}, Si_{46}, Si_{49}, and Si_{50} exhibit distinct cage-like structures. The average bond length of the inner core for Si_{41} is 2.64 Å, while for Si_{49} it decreases to 2.45 Å. Overall speaking, the average bond length in the core structures is gradually shortened as the cluster size increases, approaching the bulk Si-Si bond length, 2.352 Å. This indicates that the inner core becomes more compact. Moreover, it can be seen from Figure 3a that tetrahedron-like configuration has emerged in the core structures as embryo of bulk diamond lattice. This phenomenon can be clearly seen in the comparison of Figures 3b and 3c. The core-filling atoms partially resemble the structural characters of bulk diamond fragments. The inner cores of Si_{41}, Si_{42}, and Si_{45} have structures of square grids (see Fig. 3b), which can be compared with the structure of an adamantine along [100] lattice orientation (see Fig. 3c). Identical but less pronounced similarity was observed for Si_{50}. The structures of core-filling atoms of Si_{43} and Si_{48} contain a five-membered ring (5MR) with a top-capping silicon atom (see Fig. 3b), which closely resembles the structure of a diamantine along [110] orientation (see Fig. 3c). As shown in Figure 3b, the structures of inner cores of Si_{44}, Si_{46} and Si_{47} have a five-membered ring (5MR) with a centered silicon atom, which is very similar to the structure of diamantane along [111] orientation (see Fig. 3c). The structure of core-filling atoms of Si_{49} has character analogous to that of diamantane along [111] direction except that the structure of the inner core of Si_{49} has four broken bonds and can not form a close ring. From the above results, we may infer that the transition towards bulk structure starts from the core region of the medium-sized Si_N clusters in the size range studied. Although we only considered the endohedral fullerene with classical fullerene cages to minimize the computational efforts, the tendency of forming bulk-like fragment in the core region of medium-sized Si_N clusters should be generic and independent of the details of the configurations of outer cages.

In a previous study [33], an empirical rule for the filling/cage ratio (m/n) of endohedral fullerene cage $Si_m@Si_n$ was summarized on the basis of the results of GA-NTB global optimizations for Si_N clusters with $N = 27$–39. Considering a fullerene cage with $n = 26 + 2x$ atoms, the upper and lower limits for the number m of filling atoms should be between $3 + x$ and x. For example, in the case of $n = 36$, m can be 5 to 8, corresponding to the combinations of $Si_5@Si_{36}$ for Si_{41} to $Si_8@Si_{36}$ for Si_{44}. For $n = 38$ and 40, m can be 6 to 9 and 7 to 10, corresponding to the combinations of $Si_7@Si_{38}$ for Si_{45}, $Si_8@Si_{38}$ for Si_{46} and $Si_7@Si_{40}$ for Si_{47} to $Si_{10}@Si_{40}$ for Si_{50}, respectively.

Within a simple space-filling picture, another empirical rule [32,34] for the optimal filling/cage ratio has been proposed. Assuming a nearly spherical shape, the number m of the atoms that can be stuffed inside a fullerene cage with n surface atoms ($n = 26$–60) can be given by a simple function as

$$m \approx 0.00515n^2 + 0.03071n - 1.5525. \quad (1)$$

For $41 \leqslant n + m \leqslant 50$, equation (1) predicts $m \approx 5.88$, 6.16, 6.45, 6.74, 7.04, 7.33, 7.64, 7.94, 8.25, and 8.56, respectively, fairly close to our present results as $m = 5$, 6, 7, 8, 7, 8, 7, 8, 9, and 10. In Figure 4 we plot the number of filling atoms m as a function of the cluster size N and compare with the curves calculated from the two empirical rules. Our recent DFT results [32,35] for $30 \leqslant n+m \leqslant 40$ are also included. As shown in Figure 4, the results from DFT calculations agree well with the estimation by empirical rules in the space-filling picture.

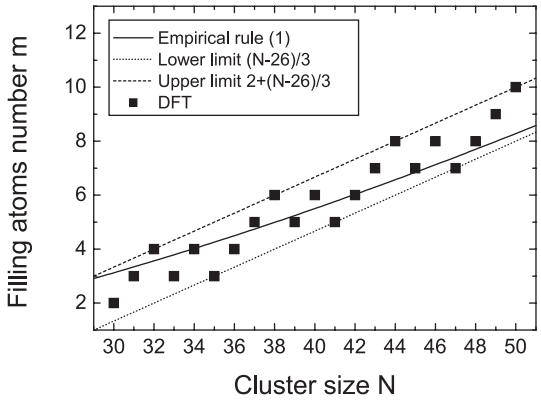

Fig. 4. Number m of atoms filling inside the spherical-like fullerene cage as a function of the cluster size N ($30 \leqslant N \leqslant 50$). For comparison, the curves calculated from two empirical rules [32,33,35] are also plotted.

4 Conclusion

In summary, we have performed a systematical search of the lowest-energy stuffed fullerene structures of silicon clusters in the size range of Si_{41}-Si_{50} using all-electron DFT calculations. For each cluster size, classical fullerene cages with different topological structures and different numbers of filling atoms have been considered. All of these energetically favorable structures are spherical-like. The optimal filling/cage combination agree well with an empirical space-filled model. The calculated binding energy and HOMO-LUMO gap of Si_{45} are larger than those of its neighbors, implying its low chemical reactivity that is consistent with the previous experiment. The core-filling atoms form cage-like geometries and the average bond lengths between the core atoms shrink as cluster becomes larger. More important, we find that the core-filling atoms exhibit structural characters that resemble bulk diamond fragments such as adamantane and diamantane. Thus, the transition towards bulk structure starts from the core region of the medium-sized Si_N clusters when the core-filling atoms gradually form cage configurations as embryo of bulk diamond lattice. Our present results indicate that Si_N ($N = 41$–50) clusters represent a unique intermediate stage of the transition from molecule-like to bulk-like behavior.

This work was supported by the National Natural Science Foundation of China (90606002, 10274031, 60478012, 10474030, 90406024) and the NCET Program provided by the Ministry of Education of China (NCET-060281).

References

1. C.C. Arnold, D.M. Neumark, J. Chem. Phys. **99**, 3353 (1993)
2. E.C. Honea, A. Ogura, C.A. Murray, K. Raghavachari, W.O. Sprenger, M.F. Jarrold, W.L. Brown, Nature **366**, 42 (1993)
3. S. Li, R.J. Van Zee, W. Weltner Jr, K. Raghavachari, Chem. Phys. Lett. **243**, 275 (1995)
4. C.S. Xu, T.R. Taylor, G.R. Burton, D.M. Neumark, J. Chem. Phys. **108**, 1395 (1998)
5. K. Raghavachari, C.M. Rohlfing, J. Chem. Phys. **89**, 2219 (1998)
6. Z.Y. Lu, C.Z. Wang, K.M. Ho, Phys. Rev. B **61**, 2329 (2000)
7. M.F. Jarrold, V.A. Constant, Phys. Rev. Lett. **67**, 2994 (1991); R.R. Hudgins, M. Imai, M.F. Jarrold, P. Dugourd, J. Chem. Phys. **111**, 7865 (1999)
8. J. Bai, L.-F. Cui, J. Wang, S. Yoo, X. Li, J. Jellinek, C. Koehler, T. Frauenheim, L.-S. Wang, X.C. Zeng, J. Phys. Chem. A **110**, 908 (2006)
9. K.A. Jackson, M. Horoi, I. Chaudhuri, T. Frauenheim, A.A. Shvartsburg, Phys. Rev. Lett. **93**, 013401 (2004)
10. S. Yoo, X.C. Zeng, J. Chem. Phys. **124**, 054304 (2006)
11. M.F. Jarrod, E.C. Honea, J. Phys. Chem. **95**, 9181 (1991)
12. T. Bachels, R. Schafer, Chem. Phys. Lett. **324**, 365 (2000)
13. K. Fuke, K. Tsukamoto, F. Misaizu, M. Sanekata, J. Chem. Phys. **99**, 7807 (1993)
14. M.A. Hoffmann, G. Wrigge, B. von issendorff, J. Muller, G. Gantefor, H. Haberland, Eur. Phys. J. D **16**, 9 (2001)
15. U. Ray, M.F. Jarrold, J. Chem. Phys. **94**, 2631 (1991); M.F. Jarrold, Y. Ijiri, U. Ray, J. Chem. Phys. **94**, 3607 (1991)
16. P. Mélinon, P. Kéghélian, B. Prével, A. Perez, G. Guiraud, J. LeBrusq, J. Lermé, M. Pellarin, M. Broyer, J. Chem. Phys. **107**, 10278 (1997)
17. P. Mélinon, P. Kéghélian, B. Prével, V. Dupuis, A. Perez, B. Champagnon, Y. Guyot, M. Pellarin, J. Lermé, M. Broyer, J.L. Rousset, P. Delichère, J. Chem. Phys. **108**, 4607 (1998)
18. Z. Iqbal, S. Veprek, J. Phys. C: Solid State Phys. **15**, 377 (1982)
19. K.M. Ho, A.A. Shvartsburg, B. Pan, Z.Y. Lu, C.Z. Wang, J.G. Wacker, J.L. Fye, M.F. Jarrold, Nature **392**, 582 (1998)
20. I. Rata, A.A. Shvartsburg, M. Horoi, T. Frauenheim, K.W.M. Siu, K.A. Jackson, Phys. Rev. Lett. **85**, 546 (2000)
21. S. Yoo, X.C. Zeng, X. Zhu, J. Bai, J. Am. Chem. Soc. **125**, 13318 (2003)
22. F.S. Khan, J.Q. Broughton, Phys. Rev. B **43**, 11754 (1991)
23. J. Song, S.E. Ulloa, D.A. Drabold, Phys. Rev. B **53**, 8042 (1996)
24. B.X. Li, P.L. Cao, J. Phys.: Condens. Matter **13**, 10865 (2001)
25. Z.F. Chen, H.J. Jiao, G. Seifert, A.H. Horn, D.K. Yu, T. Clark, W. Thiel, P.V.R. Schleyer, J. Comput. Chem. **24**, 948 (2003)
26. E. Kaxiras, Phys. Rev. Lett. **64**, 551 (1990)
27. E. Kaxiras, K. Jackson, Phys. Rev. Lett. **71**, 727 (1993)
28. D.A. Jelski, B.L. Swift, T.T. Rantala, X.F. Xia, T.F. George, J. Chem. Phys. **95**, 8552 (1991)
29. J. Pan, M.V. Ramakrishna, Phys. Rev. B **50**, 15431 (1994); M.V. Ramakrishna, J. Pan, J. Chem. Phys. **101**, 8108 (1994)
30. M. Menon, K.R. Subbaswamy, Phys. Rev. B **51**, 17952 (1995)
31. Q. Sun, Q.Wang, P. Jena, S. Waterman, Y. Kawazoe, Phys. Rev. A **67**, 063201 (2003)
32. J.L. Wang, X.L. Zhou, G.H. Wang, J.J. Zhao, Phys. Rev. B **71**, 113412 (2005)
33. S. Yoo, J.J. Zhao, J.L. Wang, X.C. Zeng, J. Am. Chem. Soc. **126**, 13845 (2004)
34. J.J. Zhao, J.L. Wang, J. Jellinek, S. Yoo, X.C. Zeng, Eur. Phys. J. D **34**, 35 (2005)
35. L. Ma, J.J. Zhao, J.G. Wang, G.H. Wang, Phys. Rev. A **73**, 063203 (2006)
36. S. Yoo, N. Shao, C. Koehler, T. Fraunhaum, X.C. Zeng, J. Chem. Phys. **124**, 164311 (2006)
37. R.L. Zhou, B.C. Pan, Phys. Rev. B **73**, 045417 (2006)
38. U. Rothlisberger, W. Anderoni, M. Parrinello, Phys. Rev. Lett. **72**, 665 (1994)
39. URL: `http://www.cochem2.tutkie.tut.ac.jp/Fuller/fsl/fsl.html`
40. DMol is a density functional theory (DFT) package based atomic basis distributed by Accelrys Inc. B. Delley, J. Chem. Phys. **92**, 508 (1990)
41. J.P. Perdew, K. Burke, M. Ernzerhof, Phys. Rev. Lett. **77**, 3865 (1996)
42. C. Kittle, *Introduction to Solid State Physics*, 7th edn. (Wiley, New York, 1996)
43. J.L. Elkind, J.M. Alford, F.D. Weiss, R.T. Laaksonene, R.E. Smally, J. Chem. Phys. **87**, 2397 (1987)
44. B. Marsen, M. Lonfat, P. Scheier, K. Sattler, Phys. Rev. B **62**, 6892 (2000)
45. J.E. Dahl., S.G. Liu, R.M.K. Carlson, Science **299**, 96 (2003)